# Nucleotides Regulate the Conformational State of the Small Terminase Subunit from Bacteriophage Lambda: Implications for the Assembly of a Viral Genome−Packaging Motor †

**ARTICLE** *in* BIOCHEMISTRY · AUGUST 2005

Impact Factor: 3.02 · DOI: 10.1021/bi050333e · Source: PubMed



**4 AUTHORS**, INCLUDING:

Helene Gaussier
Aix-Marseille Université
**11** PUBLICATIONS **190** CITATIONS
SEE PROFILE

Nasib Karl Maluf
Alliance Protein Laboratories
**43** PUBLICATIONS **946** CITATIONS
SEE PROFILE

# Nucleotides Regulate the Conformational State of the Small Terminase Subunit from Bacteriophage Lambda: Implications for the Assembly of a Viral Genome-Packaging Motor†

Hélène Gaussier,‡ Marcos E. Ortega,§ Nasib K. Maluf,‡ and Carlos E. Catalano*,‡,||

*Department of Pharmaceutical Sciences, Department of Biochemistry and Molecular Genetics, and Molecular Biology Program, University of Colorado Health Sciences Center, Denver, Colorado 80262*

*Received February 22, 2005; Revised Manuscript Received April 17, 2005*

ABSTRACT: Terminase enzymes are responsible for "packaging" of viral DNA into a preformed procapsid. Bacteriophage lambda terminase is composed of two subunits, gpA and gpNu1, in a $gpA_1$·$gpNu1_2$ holoenzyme complex. The larger gpA subunit is responsible for preparation of viral DNA for packaging, and is central to the packaging motor complex. The smaller gpNu1 subunit is required for site-specific assembly of the packaging motor on viral DNA. Terminase assembly at the packaging initiation site is regulated by ATP binding and hydrolysis at the gpNu1 subunit. Characterization of the catalytic and structural interactions between the DNA and nucleotide binding sites of gpNu1 is thus central to our understanding of the packaging motor at the molecular level. The high-resolution structure of the DNA binding domain of gpNu1 (gpNu1-DBD) was recently determined in our lab [de Beer, T., et al. (2002) *Mol. Cell 9,* 981−991]. The structure reveals the presence of a winged−helix−turn−helix DNA binding motif, but the location of the ATPase catalytic site in gpNu1 remains unknown. In this work, nucleotide binding to the gpNu1-DBD was probed using acrylamide fluorescence quenching and fluorescence-monitored ligand binding studies. The data indicate that the minimal DBD dimer binds both ATP and ADP at two equivalent but highly cooperative binding sites. The data further suggest that ATP and ADP induce distinct conformations of the dimer but do not affect DNA binding affinity. The implications of these results with respect to the assembly and function of a terminase DNA-packaging motor are discussed.

Terminase enzymes are common to many double-stranded DNA (dsDNA) viruses and are responsible for "packaging" of viral DNA into a preformed capsid (*1*, *2*). The packaging pathway is remarkably similar for viruses as distinct as the herpesviruses and many bacteriophage, and all of the characterized terminase enzymes share common structural and functional features (*1*, *3*). The terminase enzyme from bacteriophage lambda is among the best characterized and provides an ideal model system for defining the packaging mechanism for all of these viruses (*4*−*7*). Lambda terminase is composed of two subunits, gpA (640 amino acids) and gpNu1 (180 amino acids), that assemble into a functional holoenzyme complex (*8*, *9*). Recent biophysical studies indicate that the terminase protomer is a heterotrimer composed of one gpA and two gpNu1 subunits, and that this protomer further assembles into an oligomeric ring structure (*10*). We presume that the latter structure is representative of the functional holoenzyme complex assembled on viral DNA.

The preferred packaging substrate is a linear concatemer of viral genomes linked in a head-to-tail fashion generated by a rolling circle replication mechanism (*6*, *11*). The first step in DNA packaging is assembly of the terminase holoenzyme at *cos*, the junction between genomes in a concatemer (Figure 1A). An endonuclease activity in the gpA subunit nicks the duplex at *cos* to "mature" the genome end, and the binary terminase·concatemer complex binds to an empty procapsid to complete the packaging motor. This interaction activates the motor, which translocates DNA into the capsid, fueled by ATP hydrolysis at the gpA subunit.

All of the catalytic activities required to package the lambda genome reside in the gpA subunit (*12*−*18*). gpA binds to DNA nonspecifically, however, and gpNu1 is required for specific recognition of viral DNA (*1*, *19*). gpNu1 binds to three "R-elements" in the *cosB* subsite (Figure 1A) (*1*) and assembles an exceptionally stable packaging initiation complex [$T_{1/2} \approx 12$ h (*20*)]. High-affinity specific binding interactions are essential to recognition of viral DNA and maturation of the genome end prior to packaging; these specific, high-affinity interactions are provided by the terminase gpNu1 subunit (*7*). Association with the procapsid triggers "*cos* clearance", and the transition to active DNA packaging by the packaging motor. This requires that gpNu1 switch from a high-affinity assembly protein that binds specifically to *cosB* to a motor protein that binds tightly,

† This work was supported by National Institutes of Health Grant GM63943.

* To whom correspondence should be addressed: University of Colorado School of Pharmacy, 4200 E. Ninth Ave., C238, Denver, CO 80262. Phone: (303) 315-8561. Fax: (303) 315-6281. E-mail: carlos.catalano@uchsc.edu.

‡ Department of Pharmaceutical Sciences.

§ Department of Biochemistry and Molecular Genetics.

|| Molecular Biology Program.

10.1021/bi050333e CCC: $30.25 
Published on Web 06/22/2005

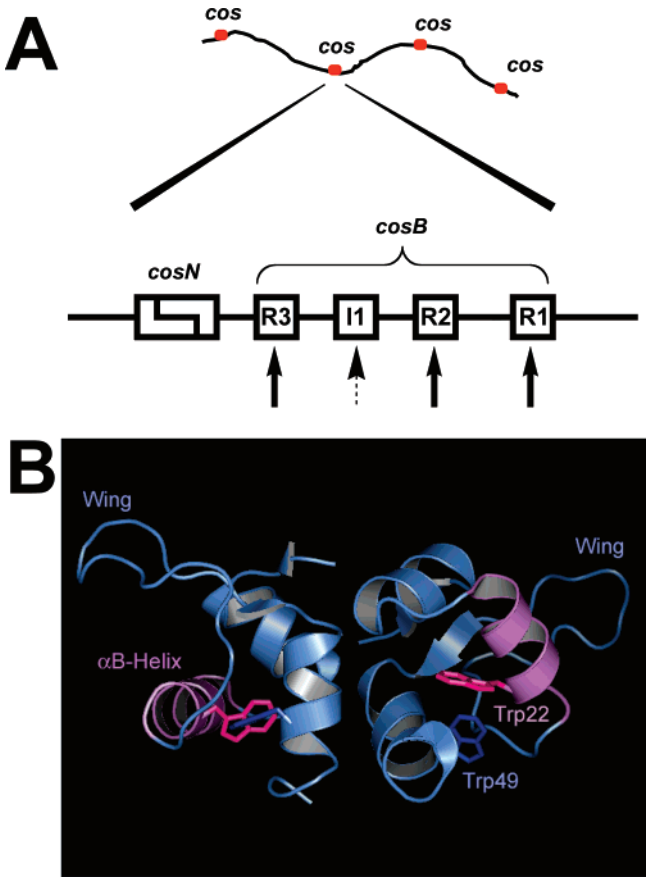


FIGURE 1: (A) λ DNA concatemer shown at the top with the *cos* sites indicated. The expansion shows the structure of the *cos* site. *CosN* is the subsite where the terminase gpA subunit cuts the duplex to mature the DNA end. The *cosB* subsite consists of three repeating R-elements (R3, R2, and R1), which represent the gpNu1 binding site (solid arrows). A consensus sequence for the *E. coli* integration host factor (I1, dashed arrow) is also found in *cosB*. gpNu1 assembly at *cosB* is required for site-specific assembly of the packaging machinery on viral DNA. (B) High-resolution NMR structure of the gpNu1-DBD dimer, taken from ref *24*. Residues 1−55 are shown in the cartoon representation looking down the dimer interface. The wing and recognition helicies (α-Helix) are indicated, with the latter colored purple. The two tryptophans in each subunit are shown in stick model representation.

but nonspecifically, to DNA to allow processive translocation of the genome into the capsid.

The gpNu1 subunit possesses an ATPase catalytic site (*16*, *21*, *22*), and allosteric interaction between the ATP and DNA binding sites has been described; ATP increases the DNA binding affinity of gpNu1, while DNA stimulates ATP hydrolysis by the subunit (*16*, *19*, *21*−*23*). On the basis of a variety of genetic and biochemical data, we have proposed that the ATPase activity of gpNu1 is required for site-specific assembly of terminase at *cos*, and that the ATP hydrolytic cycle of this subunit serves as a molecular switch that regulates specific versus nonspecific DNA binding interactions (*21*, *23*, *24*). A detailed characterization of these allosteric interactions is thus central to our understanding of the packaging motor at the molecular level.

The gpNu1 subunit is organized into three domains that have been defined by genetic and biochemical studies: (i) a C-terminal gpA interaction domain, (ii) a central self-association domain that reinforces protein−DNA interactions, and (iii) an N-terminal DNA binding domain (DBD)[1] (*1*, *25*−*28*). Primary sequence analysis suggested that a helix−turn−helix DNA binding motif (*29*) and a P-loop ATP binding motif (*30*) both reside in the N-terminal region of the protein. We therefore constructed gpNu1-E68, a construct composed of the 68 N-terminal residues of gpNu1, to provide a protein amenable to biophysical and structural analysis (*26*). Importantly, this construct is missing the self-association domain, which is responsible for aggregation of the protein at elevated concentrations. Thus, gpNu1-E68 is a soluble dimer under all conditions that were examined, and retains DNA binding activity, albeit with an affinity 3 orders of magnitude lower than that of full-length gpNu1 (*24*, *26*, *27*). The high-resolution structure of gpNu1-E68 (Figure 1B) clearly shows the presence of a winged−helix−turn−helix (wHTH) DNA binding motif, and the data establish that the gpNu1-E68 dimer is a bona fide DNA binding domain of gpNu1. Unexpectedly, however, the long-anticipated P-loop motif (*30*) is in fact the wing of the wHTH motif. This brings into question whether and where nucleotides bind to gpNu1, and whether the gpNu1 DBD retains functional ATP binding activity.

In this study, we use fluorescence spectroscopy to characterize the interaction of adenosine nucleotides with the gpNu1 DBD to determine whether this small domain also contains a functional nucleotide binding site. These studies used gpNu1-A55, a deletion construct composed of the 55 N-terminal residues of gpNu1; this construct represents the minimal folded DBD based on the solution structure of gpNu1-E68 (*24*). The effect of nucleotides and DNA on the intrinsic tryptophan fluorescence of the protein was used to monitor ligand binding and/or conformational changes induced by ligand binding. We show that (i) the gpNu1-A55 dimer contains two equivalent but highly cooperative nucleotide binding sites, (ii) ATP and ADP compete for these sites, (iii) ATP and ADP differentially affect the conformation of the dimer, and (iv) nucleotides and DNA differentially affect the conformation of gpNu1-A55. The relevance of these data to the assembly and function of a terminase DNA-packaging motor is discussed.

## EXPERIMENTAL PROCEDURES

*Materials and Methods.* Tryptone, yeast extract, and agar were purchased from DIFCO. Restriction enzymes were purchased from Promega. DEAE-Sepharose FF and SP-Sepharose FF chromatography resins were purchased from Pharmacia. [α-$^{32}$P]ATP was purchased from ICN. Unlabeled nucleoside triphosphates were purchased from Boehringer Mannheim Biochemicals. Ni−NTA agarose was purchased from Qiagen. The synthetic oligonucleotides used in this study were purchased from Invitrogen and were used without further purification. All other materials were of the highest quality commercially available.

Bacterial cultures were grown in shaker flasks utilizing a NewBrunswick Scientific series 25 incubator-shaker. All protein purifications utilized a Pharmacia FPLC system, which consisted of two P500 pumps, a GP250-plus controller,

[1] Abbreviations: AXP, ATP or ADP; AzATP, 8-azido-ATP; DBD, DNA binding domain; GDN, guanidinium hydrochloride; gpNu1-A55, deletion construct of the λ terminase gpNu1 subunit consisting of the 55 N-terminal residues of the protein; gpNu1-E68, deletion construct of the λ terminase gpNu1 subunit consisting of the 68 N-terminal residues of the protein; NLLS, nonlinear, least-squares.

a V7 injector, and a Uvicord SII variable-wavelength detector. UV−vis absorbance spectra were recorded on a Hewlett-Packard HP8452A spectrophotometer. Automated DNA sequence analysis was performed by the University of Colorado Cancer Center Macromolecular Resources Core facility. Both strands of the duplex were examined to ensure the expected DNA sequence.

*Construction of gpNu1-A55.* A truncated *Nu1* gene was amplified by PCR using pAFP1 (a generous gift of M. Feiss, The University of Iowa, Iowa City, IA) as a DNA template. This plasmid contains the wild-type *Nu1* and *A* genes cloned into a pBR322 background. Primers were designed such that *Eco*RI and *Bam*HI restriction sequences were present at the 5′ and 3′ ends, respectively, of the PCR product. A stop codon was inserted in the downstream primer sequence which yields, after amplification, a truncated *Nu1* gene that express only the first 55 amino acids of the protein. PCR amplification, isolation of the PCR product, construction of the overexpression plasmid (pNu1ΔA55), and transformation of *Escherichia coli* BL21(DE3) were performed as described previously (*26*).

*Expression and Purification of gpNu1-A55.* Four liters of terrific broth (pH 7.5) containing 50 $\mu$g/mL ampicillin was inoculated with 40 mL of an overnight culture of BL21-(DE3)[pNu1ΔA55] derived from an isolated colony. The cultures were maintained at 37 °C with vigorous agitation until an optical density ($A_{600}$) of 1.6 was obtained. IPTG was then added (1.2 mM); the culture was maintained at 30 °C for an additional 2 h, and the cells were then harvested by centrifugation (5000*g* for 15 min). All subsequent steps were preformed at 0−4 °C.

The cell pellet was resuspended in ice-cold lysis buffer [20 mM Tris-HCl buffer (pH 8) containing 100 mM NaCl, 2 mM EDTA, 7 mM 2-mercaptoethanol, 10% glycerol, 1 mM PMSF, and 10 $\mu$g/mL aprotinin]. Lysozyme (final concentration of 0.4 mg/mL) was added, and the mixture was placed on ice for 30 min. The cells were disrupted by sonication (15 bursts of 10 s each); insoluble cellular debris was removed by centrifugation (12000*g* for 30 min), and solid ammonium sulfate was added to the clarified supernatant to 15% saturation. Insoluble protein was removed by centrifugation (12000*g* for 30 min), and the supernatant was dialyzed against buffer A [20 mM Tris-HCl buffer (pH 8) containing 2 mM EDTA, 7 mM 2-mercaptoethanol, and 10% glycerol] and then loaded onto a DEAE-Sepharose column (200 mL) equilibrated with buffer A. The proteins were eluted with a 5 column volume salt gradient of 1 M NaCl from 5 to 60%; gpNu1-A55 eluted at ≈200 mM NaCl. Column fractions were examined by SDS−PAGE, and the appropriate fractions were pooled, dialyzed against buffer A, and loaded onto an SP-Sepharose column (50 mL) equilibrated with the same buffer. The proteins were eluted with a 7 column volume salt gradient of 1 M NaCl from 5 to 50%; gpNu1-A55 eluted at ≈240 mM NaCl. Column fractions were examined by SDS−PAGE, and appropriate fractions were pooled. The sample was exchanged into buffer A containing 50% glycerol and 100 mM NaCl, and concentrated using an Amicon Ultra centrifugal filter device (Millipore). The purity of the protein preparation was determined by SDS−PAGE and densitometric analysis using a Molecular Dynamics laser densitometer and the ImageQuant data analysis package, as previously described (*9*). The concentration of the purified protein was determined spectrally using an $\epsilon_{280}$ of 14 060 $M^{-1}$ $cm^{-1}$, determined by the method of Gill and von Hipple (*31*, *32*). A typical preparation yielded 15−20 mg of pure protein per liter of cell growth. The purified protein was stored at −80 °C for at least 6 months with no detectable loss of activity.

*Circular Dichroism (CD) Spectroscopy.* CD spectra were recorded on an Aviv model 62DS circular dichroism spectropolarimeter equipped with a Brinkmann Lauda RM6 circulating water bath and a thermostated cell holder. Near-UV CD spectra were acquired at 4 °C in a 0.1 cm strain-free cuvette, using a protein concentration of 1 mg/mL in 10 mM potassium phosphate buffer (pH 7.4) containing 150 mM NaCl. Data were collected between 250 and 350 nm at 1 nm intervals using a bandwidth of 1.5 nm and a dwell time of 15 s. Far-UV CD spectra were acquired at 4 °C in a 1 mm strain-free cuvette, using a protein concentration of 0.1 mg/mL. Data were collected from 180 to 250 nm at 0.5 nm intervals using a bandwidth of 1.5 nm and a dwell time of 5 s. The raw data were converted to molar ellipticity using

$$\Theta = \Theta_{obs}\left(\frac{MRW}{10bc}\right) \quad (1)$$

where $\Theta$ is the molar ellipticity (millidegrees per square centimeter per decimole), $\Theta_{obs}$ is the ellipticity recorded by the instrument (millidegrees), MRW is the mean residue weight (formula weight divided by the total number of residues in the protein), $b$ is the cell path length in centimeters, and $c$ is the protein concentration in milligrams per milliliter.

*Fluorescence Spectroscopy.* Steady-state fluorescence spectra were recorded on a Photon Technologies Quanta-Master spectrofluorometer equipped with a Masterline-Forma model 2095 circulating water bath and a thermostated cell holder maintained at 25 °C with constant stirring. The samples (3 mL) contained gpNu1-A55 (5 or 15 $\mu$M as indicated in each individual experiment) in 20 mM Tris-HCl buffer (pH 8) containing 50 mM NaCl, 2 mM EDTA, and 10% glycerol. Fluorescence emission data were collected between 305 and 400 nm using a slit width of 2 nm, a step size of 1 nm, an integration time of 5 s, and a spectrum average of 2. The excitation wavelength ($\lambda_{ex}$) was as indicated in each individual experiment.

*Acrylamide Quenching Studies.* Quenching of intrinsic tryptophan fluorescence by acrylamide was examined by sequentially adding aliquots of a 3.2 M acrylamide stock solution to 10 $\mu$M gpNu1-A55 at 25 °C. The protein solution was allowed to equilibrate with stirring for 2 min prior to the recording of the fluorescence spectrum ($\lambda_{ex}$ = 305 nm). The protein fluorescence intensity was corrected for inner filter effects due to the presence of ligand(s), and for dilution effects due to the addition of acrylamide (see eq 4 below).

Dynamic (collisional) fluorescence quenching occurs during the excited-state lifetime of the fluorophore as a result of the random collision of the quencher (Q) and the fluorophore (tryptophan) (*33*, *34*). In the absence of a static component, deactivation of the excited state is described by the Stern−Volmer equation:

$$\frac{F_o}{F} = 1 + K_{sv}[Q] \quad (2)$$

where $F_o$ and $F$ are the fluorescence intensities in the absence and presence of the quenching molecule at concentration [Q], respectively, and $K_{sv}$ is the Stern−Volmer quenching constant, the product of the bimolecular quenching rate constant and the fluorescence lifetime of the fluorophore ($K_{sv} = k_q\tau_o$). $K_{sv}$ is obtained from a plot of $F_o/F$ versus [Q], and reflects the accessibility of tryptophan to the quencher (*34*).

The fractional accessibility of protein tryptophan residues to solvent was calculated using the modified Stern−Volmer plot (Lerher plot):

$$\frac{F_o}{F_o - F} = \left(\frac{1}{[Q]}\right)\left(\frac{1}{f_a K_{sv}}\right) + \frac{1}{f_a} \quad (3)$$

where $f_a$ is the fraction of fluorophores (tryptophan) accessible to the quencher and $K_{sv}$ is the quenching constant. A plot of $F_o/(F_o - F)$ versus 1/[Q] yields $f_a$ from the *y*-intercept.

*Fluorescence-Monitored Ligand Titration*. Ligand binding to gpNu1-A55 was monitored by changes in the intrinsic tryptophan fluorescence of the protein as a function of increasing ligand concentration. Fluorescence emission was corrected for background, dilution, and the inner filter effects using eq 4 (*33*, *34*):

$$F_{corr} = (F_o - F_B)\left(\frac{v_f}{v_i}\right) \times 10^{0.5b(A_{em}+A_{ex})} \quad (4)$$

where $F_{corr}$ is the corrected fluorescence intensity, $F_o$ is the observed fluorescence of the sample, $F_B$ is the background fluorescence intensity of the buffer, $v_i$ and $v_f$ are the initial volume and final volume, respectively, of the sample after addition of the titrant, $b$ is the path length of the cell, and $A_{em}$ and $A_{ex}$ are the absorbance values of the ligand(s) at the emission and excitation wavelengths, respectively, at each point in the titration. This equation is valid for a ligand absorbance threshold of 0.05 (*34*). The fluorescence spectra were corrected for inner filter effects of all species present in solution, as appropriate.

*Analysis of Fluorescence-Monitored Ligand Binding Data.* Ligand binding data were initially analyzed using a simple binding model that assumes that each subunit in the gpNu1-A55 dimer binds a single ligand, and that binding is noncooperative between the sites. This is described by a simple Langmuir binding model

$$M + L \overset{K_L}{\longleftrightarrow} ML$$

where each subunit in the dimer (M) binds a single ligand (L). This model is described by

$$F_{obs} = \frac{S[L]}{1 + K_L[L]} + b \quad (5)$$

where $F_{obs}$ is the fluorescence intensity observed in the presence of a ligand at concentration [L], $S$ is the fluorescence signal associated with ML formation, $K_L$ is the equilibrium association constant for the interaction ($K_L = [ML]/[L][M]$), and $b$ is the baseline offset for the titration data.

The data were also analyzed using an n-site, cooperative binding model

$$M + nL \overset{K_L}{\longleftrightarrow} ML_n$$

where the two subunits in the dimer (M) bind $n$ ligands in a cooperative manner. This model is described by

$$F_{obs} = \frac{SK_L[L]^n}{1 + K_L[L]^n} + b \quad (6)$$

where $F_{obs}$ is the observed fluorescence intensity (corrected as described above) at ligand concentration [L], $S$ is the fluorescence signal associated with $ML_n$ formation, $K_L$ is the macroscopic association constant for ligand binding ($K_L = [ML_n]/[L]^n[M]$), and $b$ is the baseline offset for the titration data.

For cases where $L_{tot} \neq L_{free}$, the latter was calculated implicitly according to eq 7:

$$L_{tot} = L_{free} + n[ML_n] \quad (7)$$

*Analysis of the ATP Competitive Binding Data.* ADP and ATP-$\gamma$S induce a change in the intrinsic fluorescence of gpNu1-A55, but ATP does not (see the text). Competition experiments were conducted to determine if ATP could compete for ADP and/or ATP-$\gamma$S binding to gpNu1-A55. These experiments considered a simple competitive binding model (Scheme 1):

Scheme 1

$$M + 2L \overset{K_L}{\longleftrightarrow} ML_2$$

$$M + 2T \overset{K_T}{\longleftrightarrow} MT_2$$

where M is the gpNu1-A55 dimer, $ML_2$ represents the dimer bound to two "ligand" molecules (in this case ADP or ATP-$\gamma$S), and $MT_2$ represents the dimer bound to two molecules of ATP. This simple model assumes that (i) the gpNu1 dimer contains two equivalent but cooperative binding sites, (ii) ligand binding to gpNu1 induces a fluorescence change but ATP does not, (iii) ligand and ATP compete for the same binding sites, and (iv) the heterocomplex (i.e., a dimer bound to one ligand and one ATP each) is not significantly populated at equilibrium. This simple competition model is described by

$$F_{obs} = \frac{SK_L[L]^2}{1 + K_L[L]^2 + K_T[T]^2} + b \quad (8)$$

where $F_{obs}$ is the observed fluorescence signal in the presence of ligand (ADP or ATP-$\gamma$S) at concentration [L] and ATP at concentration [T], $S$ is the fluorescence signal associated with $ML_2$ species, and $b$ is the baseline resulting from ATP competition of ligand binding. $K_L$ is the macroscopic association constant for ligand binding ($K_L = [M{\cdot}L_2]/[L]^2[M]$), and $K_T$ is the macroscopic association constant for ATP binding ($K_T = [M{\cdot}T_2]/[T]^2[M]$).

For cases where $L_{tot} \neq L_{free}$ and $T_{tot} \neq T_{free}$, $L_{free}$ and $T_{free}$ were calculated implicitly according to eqs 9 and 10:

$$L_{tot} = L_{free} + 2[ML_2] \quad (9)$$

$$T_{tot} = T_{free} + 2[MT_2] \quad (10)$$

The ATP competition experiments were performed in the presence of three different concentrations of ADP. A global analysis of all three data sets, in addition to the ADP binding data, was performed according to the model presented in Scheme 1 to generate the binding constants presented in this work. The competition of ATP with ATP-$\gamma$S was analyzed identically. Mathematical analyses and modeling of the binding data were performed using Scientist.

*Affinity Labeling of A55 with 8-Azido-ATP (AzATP).* A typical photoaffinity labeling experiment utilized 50 $\mu$M gpNu1-A55 in 15 $\mu$L of binding buffer [50 mM Tris-HCl buffer (pH 9) containing 10 mM $MgCl_2$, 10 mM NaCl, 5 nM $\lambda$ DNA, and 50 $\mu$M [$\alpha$-$^{32}$P]AzATP (0.2 $\mu$Ci/nmol)]. Nucleotides were added to a concentration of 1 mM, as indicated. The mixture was kept on ice for 3 min and then illuminated for 2 min with a hand-held UV lamp (254 nm at a distance of 4 cm). The reaction was stopped with the addition of an equal volume of quench buffer (100 mM EDTA and 10 mM DTT), and the protein was fractionated by 15% SDS−PAGE. The gpNu1-A55 protein band was stained with Coomassie blue, and radioactive bands were visualized by phosphorimage analysis using a Molecular Dynamics Storm system.

## RESULTS

We previously described the biochemical, biophysical, and structural properties of gpNu1-E68, a construct that encompasses the DNA binding domain (DBD) of the small subunit of lambda terminase (*27*). The protein forms a stable dimer in the concentration range of 5 $\mu$M to 2 mM with no evidence for dissociation or further self-association. Biophysical studies (*27*) and the high-resolution structure of gpNu1-E68 (*24*) reveal that the C-terminal residues of the construct adopt a pseudostable helical structure. On the basis of these data, we constructed gpNu1-A55, a construct in which these partially ordered residues have been deleted from the protein. gpNu1-A55 thus represents the minimal DNA binding domain of gpNu1.

*Characterization of gpNu1-A55.* gpNu1-A55 expressed in *E. coli* and purified as described in Experimental Procedures yields 15−20 mg of purified protein per liter of cell culture. The protein preparation was judged to be >95% homogeneous as determined by SDS−PAGE and densitometric analysis, and was essentially devoid of contaminating nucleic acids as determined by UV−vis spectroscopy ($A_{280}/A_{260}$ = 1.93) (data not shown). Analysis of the far-UV CD spectrum of gpNu1-A55 (Figure 2A) indicates that the protein contains 29% $\alpha$-helix and 22% $\beta$-sheet structures, similar to the values of gpNu1-E68 (*27*). The near-UV CD spectrum of gpNu1-A55 (Figure 2B) is identical to that of gpNu1-E68, as expected, since no aromatic residues were deleted.

Figure 2C shows the thermal denaturation profile for gpNu1-A55 monitored by CD spectroscopy. It is noteworthy that the denaturation profiles are identical whether they are monitored at 222 nm (a measure of secondary structure) or 296 nm (a measure of tertiary structure). This is in contrast to the situation observed with gpNu1-E68 (and larger deletion

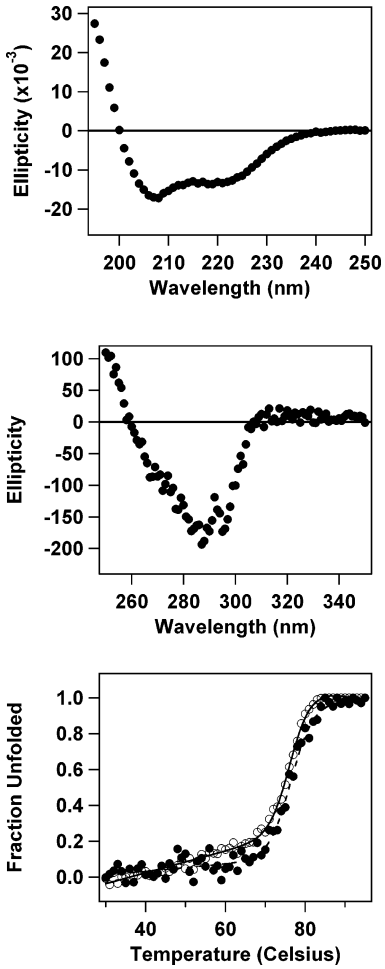


FIGURE 2: Circular dichroic spectra of gpNu1-A55. Panels A and B show the far-UV and near-UV CD spectra of gpNu1-A55, respectively. Panel C shows the thermally induced denaturation of gpNu1-A55. Unfolding of gpNu1-A55 was monitored by far-UV (●) and near-UV (○) CD signals as described in Experimental Procedures.

constructs), where secondary structure elements "melted" prior to global unfolding of the protein. We proposed that this unusual observation resulted from "unraveling" of the C-terminal pseudostable helix prior to unfolding of the protein core, and loss of tertiary structure (*27*). Consistent with this suggestion, deletion of the pseudostable helix in gpNu1-A55 yields a construct in which global unfolding of the protein results in simultaneous loss of secondary and tertiary structures. We further note that the $T_m$ for thermal denaturation of gpNu1-A55 (75.6 ± 0.6 °C) is significantly greater than that of gpNu1-E68 (63.3 ± 0.3 °C) (*27*). This surprising observation indicates that the pseudostable helix (residues 56−68) influences the thermal stability of the folded core of the protein, and that deletion of this partially ordered helix strongly stabilizes the folded core. Like gpNu1-E68 (*27*), gpNu1-A55 forms a soluble, stable dimer in the concentration range of 3−15 $\mu$M, as determined from sedimentation equilibrium studies (data not shown). Neither ADP nor ATP affects the self-association behavior of the protein (data not shown).

*Fluorescence Analysis of gpNu1-A55.* These experiments used an excitation wavelength of 305 nm to ensure that tryptophan fluorescence is selectively observed in the spectrum, which yielded a peak of fluorescence intensity ($\lambda_{em,max}$) at 336 nm. The position of $\lambda_{em,max}$ suggests that all

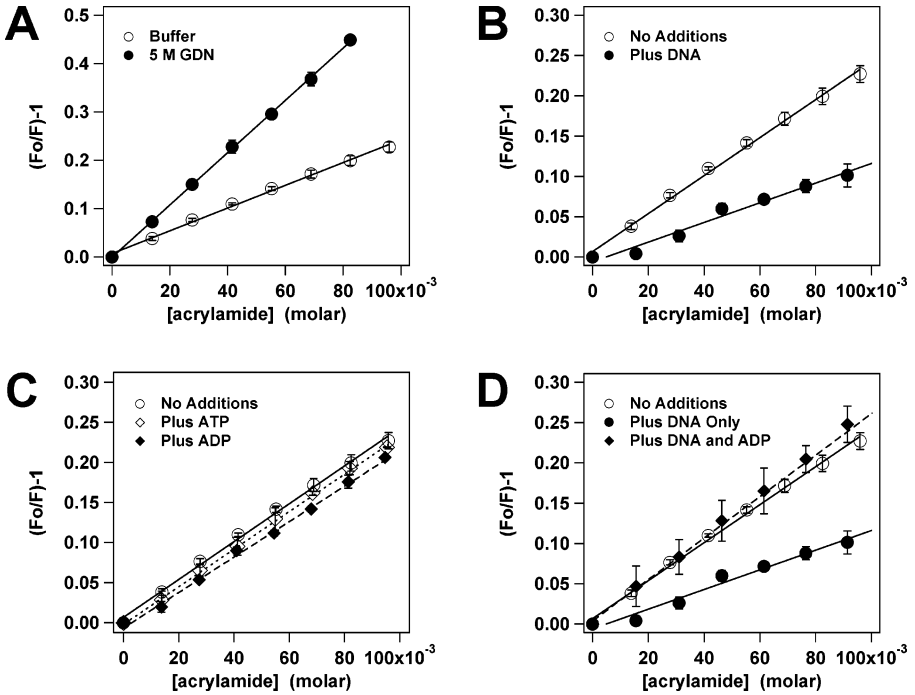


FIGURE 3: Acrylamide quenching of gpNu1-A55 intrinsic tryptophan fluorescence. Fluorescence spectra were recorded in the presence of increasing concentrations of acrylamide as described in Experimental Procedures. The concentration of gpNu1-A55 is 10 $\mu$M, and $\lambda_{ex}$ = 305 nm. Each data point represents the average of three separate experiments; error bars represent the standard deviation. (A) Spectra were recorded in the absence (○) or presence (●) of 5 M guanidinium hydrochloride. (B) Spectra were recorded in the absence (○) or presence (●) of 30 $\mu$M R3, a 14 bp DNA duplex corresponding to the R3 gpNu1 recognition element (see Figure 1A). (C) Spectra were recorded in the absence of nucleotides (○), in the presence of 1 mM ATP (◇), or in the presence of 1 mM ADP (◆). (D) Spectra were recorded in the absence of nucleotides or DNA (○), in the presence of 30 $\mu$M R3 DNA alone (●), or in the presence of 30 $\mu$M R3 DNA and 1 mM ADP (◆). Identical results were obtained in the presence of 30 $\mu$M R3 DNA and 1 mM ATP (see Table 1). We note that DNA could not be added at a concentration sufficient to saturate the DNA binding site (see Figure 4A) because of strong inner filter effects.

four tryptophan residues in the gpNu1-A55 dimer reside in a hydrophobic environment, as expected from structural data (see Figure 1B). Denaturation of gpNu1-A55 with guanidinium hydrochloride (GDN) results in a red shift in $\lambda_{em,max}$ (to 350 nm), and an increase in fluorescence intensity (not shown). This is consistent with the observation that the tryptophan residues are buried, at least in part, in the folded protein, but become exposed to solvent upon denaturation in GDN (*35*). Identical results were obtained with the gpNu1-E68 construct (*27*).

*Acrylamide Quenching of the Intrinsic Fluorescence of gpNu1-A55.* Addition of acrylamide to gpNu1-A55 quenches the intrinsic fluorescence of the protein. The effect of acrylamide concentration on gpNu1-A55 tryptophan fluorescence was quantified using a Stern−Volmer analysis of the quenching data (Figure 3A). The linear character of the Stern−Volmer plot and the observation that acrylamide affects the quantum yield but does not affect the $\lambda_{em,max}$ of the protein fluorescence spectrum suggest that a single class of tryptophan residues is affected by the quencher (*34*).

Denaturation of gpNu1-A55 exposes the protein tryptophans to solvent (vide supra), and the acrylamide quenching constant ($K_{sv}$, the slope of the Stern−Volmer plot) is, as expected, significantly greater in the presence of 5 M GDN (Figure 3A and Table 1). Analysis of the data using a modified Stern−Volmer (Lerher) plot indicates that the fractional accessibility of tryptophan is 52% in the natively folded protein and 100% in the denatured protein (Table 1). This indicates that either (i) only two of the four tryptophan residues in the gpNu1-A55 dimer are accessible to acrylamide in the native state or (ii) each of the four tryptophans is partially solvent exposed. The solution structure of gpNu1-A55 suggests that the latter explanation is correct (see Figure 1B).

Table 1: Acrylamide Quenching of gpNu1-A55 Intrinsic Tryptophan Fluorescence[a]

| additions | $K_{sv}$ ($M^{-1}$) | $f_a$ (%) |
|---|---|---|
| none | 2.28 ± 0.01 | 52.2 ± 3.5 |
| 5 M GDN | 5.42 ± 0.01 | 100.8 ± 1.2 |
| 1 mM ADP | 2.23 ± 0.01 | 57.3 ± 4.9 |
| 1 mM ATP | 2.26 ± 0.01 | 56.6 ± 4.8 |
| 30 $\mu$M DNA | 1.1 ± 0.01 | 26.5 ± 1.3 |
| 30 $\mu$M DNA and 1 mM AMP | 1.1 ± 0.01 | ND[b] |
| 30 $\mu$M DNA and 1 mM ADP | 2.52 ± 0.01 | 58.7 ± 5.3 |
| 30 $\mu$M DNA and 1 mM ATP | 2.54 ± 0.01 | 50.4 ± 4.2 |

[a] The data presented in Figure 3 were analyzed as described to calculate the Stern−Volmer constant ($K_{sv}$) and fractional tryptophan accessibility ($f_a$). [b] Not done.

*Effect of DNA and Nucleotides on Acrylamide Quenching of gpNu1-A55 Tryptophan Fluorescence.* The gpNu1 subunit is responsible for terminase assembly at the packaging initiation site in the lambda genome (*20*). This is accomplished by specific recognition of three R-elements in viral DNA by the winged−helix−turn−helix motif in gpNu1 (see Figure 1). Gel mobility shift assays demonstrate that gpNu1-A55 binds to a 272 bp *cos*-containing duplex with an affinity similar to that of gpNu1-E68 ($C_{1/2} \approx 50$ $\mu$M; data not shown). Unfortunately, the 272 bp DNA substrate is too large for use in fluorescence studies; we therefore used a 14 bp duplex representing the sequence of the R3 element to examine the effect of DNA on acrylamide quenching of protein fluorescence. Figure 3B shows that this short duplex

significantly affects acrylamide quenching of the protein, resulting in a significant decrease in both $K_{sv}$ and the fractional solvent accessibility of tryptophan (see Table 1). This suggests that DNA binds to gpNu1-A55, and that acrylamide has restricted access to tryptophan residues in the binary protein·DNA complex; we presume that this is due to a conformational change in the dimer structure. Of note is the fact that a 14 bp duplex representing the sequence of R4 (nonspecific DNA[2]) yields similar results (data not shown).

The gpNu1 subunit possesses ATPase activity, but the location of the ATPase catalytic site in the protein remains obscure (see the introductory section and ref *24*). As an initial probe for nucleotide binding to gpNu1-A55, we examined the effect of nucleotides on acrylamide quenching of tryptophan fluorescence. Figure 3C shows that neither ATP nor ADP significantly influences acrylamide quenching of gpNu1-A55. Interestingly, however, ATP and ADP both abrogate the observed decrease in the Stern−Volmer slope induced by the presence of DNA alone (Figure 3D and Table 1). This effect is not observed with AMP (Table 1), which suggests that ATP and ADP specifically interact with gpNu1-A55, but that AMP does not. The data further suggest that AXP and DNA differentially affect the conformation of the gpNu1-A55 dimer. This is examined more fully below.

*Fluorescence-Monitored Ligand Binding by gpNu1-A55*. Previous NMR experiments demonstrated that gpNu1-E68 binds to a 16 bp duplex that represents the sequence of the R3 element (*24*). Here we examine DNA binding to gpNu1-A55 using fluorescence spectroscopy. These studies utilized 14 bp duplexes that represent the R3 (specific) and R4 (nonspecific) elements of lambda DNA (described above). Both duplexes strongly quench the intrinsic tryptophan fluorescence of gpNu1-A55 in a concentration-dependent manner (Figure 4A) but do not affect $\lambda_{em,max}$ (not shown). Unfortunately, an accurate analysis of the data is not possible due to significant inner filter effects of the DNA substrate at concentrations greater than 40 $\mu$M, which precludes saturation of the DNA binding site. The data nevertheless indicate that gpNu1-A55 binds these short duplexes weakly and nonspecifically; weak binding to a 16 bp duplex was similarly observed in the NMR-monitored titration experiments (*24*). Interestingly, Figure 4B shows that nucleotides do not affect the apparent binding affinity of these short duplexes for gpNu1-A55.

The data presented in Figure 3D and Table 1 suggest that both ATP and ADP bind to gpNu1-A55. To directly test this hypothesis, we performed fluorescence-monitored nucleotide titration experiments. Unexpectedly, ATP at concentrations as high as 1.6 mM does not significantly affect the intrinsic tryptophan fluorescence of the protein (Figure 5A). In contrast, addition of either ADP or ATP-$\gamma$S results in a small but highly reproducible quenching of the intrinsic tryptophan fluorescence in a concentration-dependent manner (Figure 5B). This unusual effect is investigated further below.

*Photolabeling of gpNu1-A55 with AzATP*. We next examined photoaffinity labeling of gpNu1-A55 with the ATP analogue AzATP. These experiments demonstrate that gpNu1-A55 is covalently modified by AzATP in the presence of UV light (Table 2). Importantly, prephotolyzed AzATP does not modify the protein, and photolabeling is competitive with adenosine nucleotides. ATP and ADP inhibit photolabeling by 85 and 65%, respectively, while AMP has a modest effect (Table 2). The errors associated with these values are large (≈15%), but the data nevertheless indicate that AzATP binds to a specific nucleotide-binding site located within the gpNu1-A55 dimer.

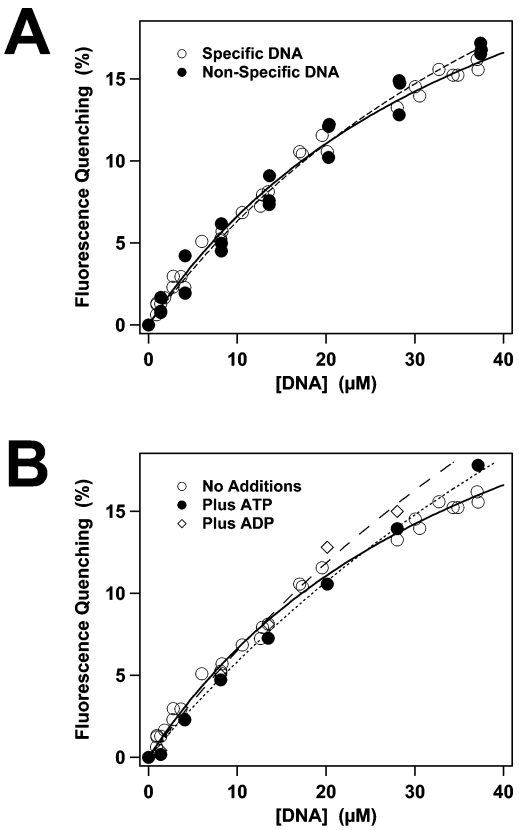


FIGURE 4: Fluorescence-monitored DNA binding to gpNu1-A55. (A) The intrinstic tryptophan fluorescence of gpNu1-A55 (10 $\mu$M, $\lambda_{ex}$ = 305 nm) was recorded in the presence of increasing concentrations of specific R3 DNA (○) or nonspecific R4 DNA (●) as described in Experimental Procedures. (B) Fluorescence-monitored titration of gpNu1-A55 with R3 DNA in the absence of nucleotide (○), in the presence of 1 mM ATP (●), or in the presence of 1 mM ADP (◇). Essentially identical results were obtained with AMP.

*ATP Binding to gpNu1-A55*. The results presented above show that AzATP covalently modifies gpNu1-A55 in the presence of UV light, and that ATP and ADP both compete for the AzATP binding site. These data strongly suggest that ATP binds to a specific nucleotide binding site in gpNu1-A55. Therefore, fluorescence-monitored competitive binding experiments were performed as a direct probe of ATP binding. Figure 5B demonstrates that ADP binds to gpNu1-A55 and quenches the intrinsic tryptophan fluorescence of the protein. We reasoned that ATP binding to the ATPase catalytic site should compete with ADP and affect the fluorescence intensity of the protein·ADP complex (see Scheme 1). In this experiment, gpNu1-A55 was preincubated with ADP and the fluorescence intensity of the complex monitored upon titration with ATP. The experiment was repeated at three different ADP concentrations (0.5, 1.6, and 3 mM), and the results are presented in Figure 6A. The data clearly show that ATP reverses quenching by ADP in a concentration-dependent manner, a result consistent with

[2] R4 represents an element that is similar in sequence to R3 but that is not bound by gpNu1.

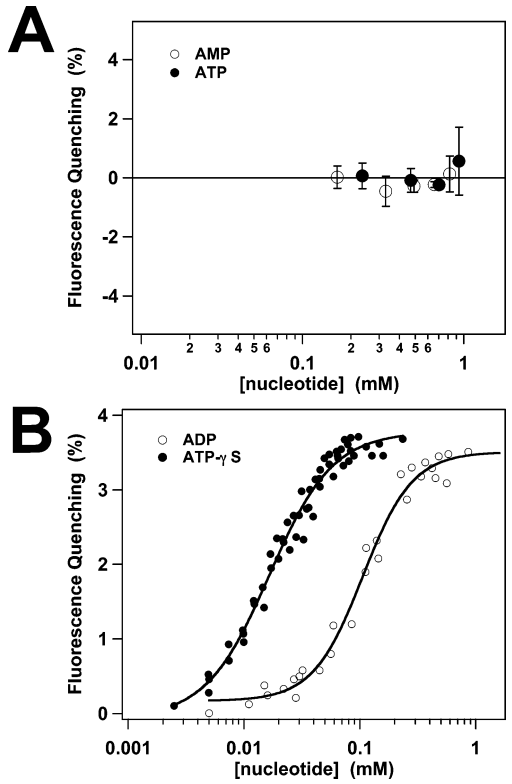


FIGURE 5: Fluorescence-monitored nucleotide binding to gpNu1-A55. (A) The intrinsic tryptophan fluorescence of gpNu1-A55 was recorded in the presence of increasing concentrations of ATP (●) or AMP (○), as indicated. Each data point represents the average of three separate measurements; error bars show the standard deviation. (B) The intrinsic tryptophan fluorescence of gpNu1-A55 (5 $\mu$M, $\lambda_{ex}$ = 295 nm) was recorded in the presence of increasing concentrations of ADP (○) or ATP-$\gamma$S (●), as indicated. The ensemble of data obtained in three separate titration experiments is displayed. The solid lines represent the best fit of the data from a global analysis of the binding data presented here and the competition data presented in Figure 6. The macroscopic binding constants derived from this analysis are listed in Table 4.

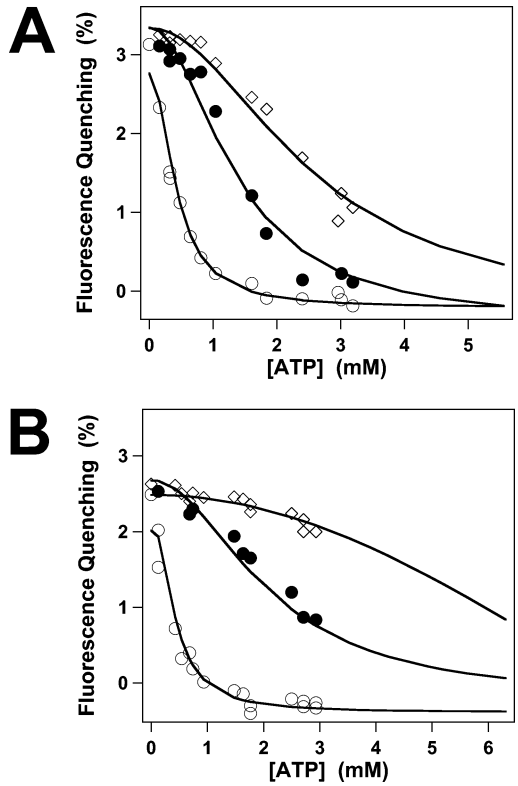


FIGURE 6: ATP competes with ADP and ATP-$\gamma$S for the nucleotide binding site. (A) ATP was incrementally added to 5 $\mu$M gpNu1-A55 preincubated with 0.5 mM ADP (○), 1.6 mM ADP (●), or 3 mM ADP (◇), as indicated, and intrinsic tryptophan fluorescence monitored. The solid lines represent the best fit of the data from a global analysis of the competitive binding data presented here and the direct binding data presented in Figure 5B. The macroscopic binding constants derived from this analysis are listed in Table 4. (B) ATP was incrementally added to gpNu1-A55 preincubated with 0.1 (○), 0.5 (●), or 3.5 mM ATP-$\gamma$S (◇), as indicated, and intrinsic tryptophan fluorescence monitored. The solid lines represent the best fit of the data from a global analysis of the competitive binding data presented here and the direct binding data presented in Figure 5B. The macroscopic binding constants derived from this analysis are listed in Table 4. An excitation wavelength of 305 nm was used in the presence of elevated concentrations of nucleotides (3 mM ADP or 3.5 mM ATP-$\gamma$S) to minimize inner filter effects.

Table 2: Photoaffinity Labeling of gpNu1-A55 with AzidoATP[a]

| reaction modification | relative labeling efficiency (%) |
|---|---|
| none | 100 |
| plus 1 mM AMP | 80 ± 18 |
| plus 1 mM ADP | 35 ± 16 |
| plus 1 mM ATP | 15 ± 14 |
| prephotolyzed AzATP | 0 |

[a] AzATP was photolyzed in the presence of gpNu1-A55 and the extent of covalent modification quantified as described in Experimental Procedures. Labeling in the absence of nucleotides was taken to be 100%. The data represent the average and standard deviation of the experiment performed in triplicate; 0% indicates no detectable photoaffinity labeling was observed.

competitive binding by the nucleotides. Figure 5B demonstrates that ATP-$\gamma$S also binds to gpNu1-A55 and quenches the intrinsic tryptophan fluorescence of the protein; competition experiments between ATP and ATP-$\gamma$S (0.1, 0.5, and 3.5 mM) yield results identical to those obtained with ADP (Figure 6B). Importantly, AMP at concentrations up to 1.5 mM does not affect the intrinsic fluorescence intensity of the protein·ADP complex (not shown).

*Analysis of the Nucleotide Binding Data.* The ADP binding data presented in Figure 5B were analyzed using a Langmuir binding model (eq 5) as described in Experimental Procedures; the data are poorly described by this simple model in the nonlinear, least-squares (NLLS) analysis (not shown). Given that gpNu1-A55 is a symmetric dimer that presumably contains two ATP binding sites (see Figure 1), we next analyzed the data using a two-site binding model. Initially, we assumed that the two sites are identical but highly cooperative (a Hill model, eq 6). NLLS fitting of the data to this model yielded a reasonable fit, which returned two sites ($n$ = 2.0 ± 0.2) and a macroscopic equilibrium association constant ($K_A$) of 96 ± 53 mM$^{-2}$ (Table 3). A similar analysis of the ATP-$\gamma$S binding data was also consistent with two sites ($n$ = 1.7 ± 0.2) and returned a $K_A$ of 856 ± 545 mM$^{-2}$ (Table 3). While the errors associated with these values are

Table 3: Analysis of the Nucleotide Binding Data[a]

| | ADP | ATP-$\gamma$S |
|---|---|---|
| $K_A$ (mM$^{-2}$) | 96 ± 53 | 856 ± 545 |
| no. of ADP binding sites ($n$) | 2.0 ± 0.2 | 1.7 ± 0.2 |
| goodness of fit | 0.17 | 0.16 |

[a] The data presented in Figure 5 were analyzed by NLLS methods as described in Experimental Procedures.

Table 4: Global Analysis of the Nucleotide Binding Data[a]

| | ADP competition | ATP-$\gamma$S competition |
|---|---|---|
| $K_A$(competitor) | $K_{A,ADP} = 90 \pm 11$ mM$^{-2}$ | $K_{A,ATP-\gamma S} = 3158 \pm 268$ mM$^{-2}$ |
| $K_{A,ATP}$ | $K_{A,ATP} = 126 \pm 20$ mM$^{-2}$ | $K_{A,ATP} = 180 \pm 30$ mM$^{-2}$ |
| goodness of fit | 0.13 | 0.48 |

[a] The ensemble of data presented in Figures 5 and 6 were globally fit as described in Experimental Procedures. The results of the NLLS analysis are displayed as solid curves in Figures 5 and 6.

large,[3] it is clear that ATP-$\gamma$S binds with greater affinity than ADP, and that both nucleotides bind in the micromolar range. Analysis of the data using other models (i.e., two nonequivalent binding sites) did not improve the quality of the NLLS fitting (not shown).

*Analysis of the Competitive Nucleotide Binding Data*. The data presented above suggest that ATP binds to gpNu1-A55 but does not affect the intrinsic tryptophan fluorescence of the protein. This precludes a direct evaluation of ATP binding affinity using fluorescence titration methods; however, the fluorescence-monitored competitive binding data may be analyzed to extract this information, as described in Experimental Procedures. The simple model described in Scheme 1 assumes that (i) the gpNu1 dimer contains two equivalent but highly cooperative binding sites, (ii) binding of the ligand to gpNu1 induces a fluorescence change but that ATP does not, (iii) ligand and ATP compete for the same binding sites, and (iv) the heterocomplex (i.e., a dimer bound to one ADP and one ATP each) is not significantly populated at equilibrium. The ensemble of data presented in Figure 6A (ATP titration profiles in the presence of three different concentrations of ADP) and the ADP binding data presented in Figure 5B were analyzed in a single, global NLLS fit to the simple competitive binding model (see eq 8). This analysis provides a good fit to the data, and the results are presented in Figure 5B (solid line on the ADP binding data) and as the series of curves presented in Figure 6A (the competition data). A similar analysis of the ATP-$\gamma$S competitive binding data also yields a good fit (solid line in Figure 5B and a series of lines in Figure 6B). The macroscopic equilibrium association constants for both analyses are presented in Table 4, which provides a $K_{A,ATP}$ of $126 \pm 20$ mM$^{-2}$ in the global analysis of the ADP data and a $K_{A,ATP}$ of $180 \pm 30$ mM$^{-2}$ in the global analysis of the ATP-$\gamma$S data. It is noteworthy that the $K_{A,ATP}$ values returned from both experiments are quite similar (Table 4), which is predicted by the simple competition model. Analysis of the data using more complicated models (i.e., the presence of a heteroligated species such as dimer·ATP·ADP) does not improve the quality of the fit (not shown). Thus, the fractional population of a putative heteroligated species is predicted to be small.

[3] The value of *n* was allowed to "float" in the NLLS analysis of the data to provide an experimental estimate of the number of nucleotide binding sites in the dimer. Unfortunately, this results in large errors associated with the estimate of $K_A$. We attempted to perform a stoichiometric binding experiment to directly measure the number of ATP molecules that bind to a gpNu1-A55 dimer. On the basis of the estimated $K_A$, this experiment requires elevated concentrations of the protein ($>1$ $\mu$M). Unfortunately, aggregation of the protein under these conditions precluded the analysis.

## DISCUSSION

The small terminase subunit, gpNu1, is responsible for site-specific assembly of the DNA-packaging machinery at *cos*, the packaging initiation site in a lambda concatemer (*1*, *6*−*9*, *20*). DNA binding by gpNu1 is modulated by ATP, and the subunit possesses an ATPase activity that is stimulated by DNA (*16*, *20*−*24*, *36*). Allosteric interaction between the DNA and ATP binding sites in gpNu1 is thus evident, and these interactions likely modulate the assembly, stability, and activity of the packaging motor complex (*1*, *23*). Characterization of these interactions at both the biochemical and structural level is central to a molecular description of viral DNA packaging. We therefore examined nucleotide binding to a minimal DNA binding domain of gpNu1 to determine whether the construct also contains a functional nucleotide binding site.

*Characterization of gpNu1-A55, the Minimal DNA Binding Domain of gpNu1*. The high-resolution structure of gpNu1-E68 reveals that the 10−13 C-terminal residues of the construct form an unstable, extended helix that is not part of the folded core of the protein (*24*). We therefore constructed a vector that expresses gpNu1-A55, a deletion construct that encompasses the 55 N-terminal residues of gpNu1. The spectral and physical properties of gpNu1-A55 are indistinguishable from those of gpNu1-E68, and indicate that the shorter construct is soluble and appropriately folded in solution. Moreover, gpNu1-A55 retains a dimeric structure under all conditions that were examined and binds to *cos* DNA with an affinity similar to that of gpNu1-E68. The ensemble of data demonstrates that gpNu1-A55 represents the folded core of gpNu1-E68 and encompasses the minimal DNA binding domain of the small terminase subunit. We therefore use the term gpNu1-DBD to denote the entirety of gpNu1-A55, and the folded core of gpNu1-E68.

Tryptophan residues may be used as fluorescent probes to investigate the dynamic nature of a protein (*34*). Intrinsic protein fluorescence may be quenched by acrylamide, and the extent of quenching is an indication of the level of exposure of tryptophan to solvent. The gpNu1-A55 dimer possesses four tryptophans, and as expected, 100% of the tryptophan fluorescence signal is accessible to acrylamide when the protein is denatured in GDN. Conversely, only 50% of the fluorescence signal is accessible in natively folded gpNu1-A55. This observation is consistent with the solution structure of the DBD, which indicates that all of the tryptophans are partially buried in the folded dimer structure (see Figure 1).

*Cooperative Nucleotide Binding by gpNu1-A55*. Our data show that ADP binds to gpNu1-A55 and quenches the intrinsic tryptophan fluorescence of the protein. The data are described well by a model in which the dimer contains two equivalent nucleotide binding sites that interact in a highly cooperative manner. ATP-$\gamma$S also binds to the protein, but with significantly greater affinity. Thus, the minimal DBD of gpNu1 also retains a functional nucleotide-binding site. Given that gpNu1 possesses ATPase activity, it was initially disappointing that ATP did not affect protein fluorescence. Nevertheless, direct competition experiments clearly show that (i) ATP binds to gpNu1-A55, (ii) ATP and ADP compete for the same binding site(s), and (iii) both nucleotides bind with similar affinities. We note that both nucleotides bind

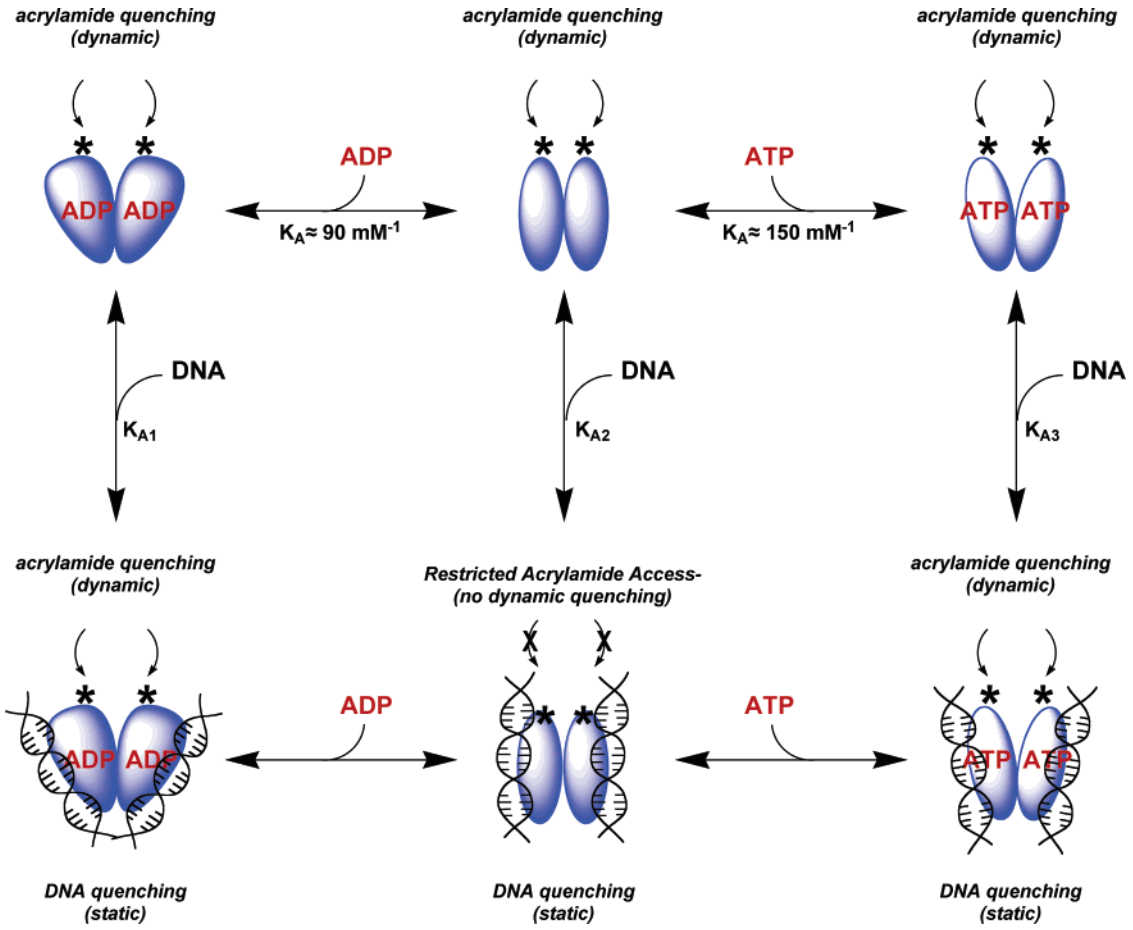


FIGURE 7: Model for DNA and nucleotide binding interactions. Acrylamide quenches the intrinsic tryptophan fluorescence of gpNu1-A55 (dynamic quenching). DNA binds to the two wHTH motifs in the dimer (center) and directly quenches intrinsic fluorescence (static quenching). Access of acrylamide to the tryptophan residues is restricted in the binary DNA·gpNu1-A55 complex, and dynamic quenching is not observed. ATP and ADP bind to gpNu1-A55 and induce slightly different conformations of the dimer structure (top), which does not affect DNA binding affinity ($K_{A1} \approx K_{A2} \approx K_{A3}$). The putative conformational changes yield an "open" structure, however, where acrylamide again has unrestricted access to tryptophans at the dimer interface.

to gpNu1-A55 in the mid-micromolar range, which is consistent with the observed $K_M$ of ≈500 $\mu$M for ATP hydrolysis by gpNu1[4] (*21*, *22*). This latter observation suggests that ATP binding affinity is fully retained in the minimal DBD. Finally, we emphasize that while both nucleotides can bind to gpNu1-A55, ADP binding quenches protein fluorescence but ATP does not. This suggests that either (i) ATP and ADP bind to the nucleotide binding site in unique orientations or (ii) the two nucleotides induce different conformations of the dimer. gpNu1 binds and hydrolyzes ATP to ADP (*21*, *22*), and it is unlikely that the catalytic site would bind the two nucleotides in significantly different orientations. We therefore favor the latter explanation. This is discussed in more detail below.

*DNA Binding by gpNu1-A55*. Fluorescence-monitored titration studies show that a 14 bp duplex binds to gpNu1-A55 and strongly quenches the intrinsic tryptophan fluorescence of the protein. DNA binding is also evident in the acrylamide quenching studies, as follows. In the presence of DNA, acrylamide quenching of protein fluorescence is strongly attenuated, as indicated by a significant decrease in the slope ($K_{sv}$) of the Stern−Volmer plot. This could result from a number of mechanisms.[5] First, DNA binding could directly occlude tryptophan residue(s) from the solvent and thus restrict access to acrylamide; however, this mechanism predicts a curved Stern−Volmer plot (*34*, *37*), which is not observed. Second, DNA binding could drive a change in the conformation of the dimer, which further sequesters tryptophan residue(s) from solvent. Within this context, we note that DNA binding to gpNu1-A55 quenches the intrinsic tryptophan fluorescence, but does not affect the $\lambda_{em,max}$. Thus, if DNA binding does induce a conformational change in dimer structure, the local environment surrounding the tryptophan residues is not significantly altered. The latter suggestion is consistent with NMR-monitored titration studies (*24*). Unfortunately, our data do not allow a mechanistic interpretation; nevertheless, both the acrylamide quenching experiments and direct monitoring of protein fluorescence indicate that short DNA duplexes bind weakly to gpNu1-A55.

*Nucleotide-Induced Conformational Changes?* ATP, ADP, and ATP-$\gamma$S bind to gpNu1-A55, but do not affect acrylamide quenching of the dimer. Thus, acrylamide access to

[4] The isolated gpNu1 subunit does not possess ATPase activity. The indicated $K_M$ is for ATP hydrolysis by full-length gpNu1 in the context of the holoenzyme and in the presence of DNA. In the absence of DNA, the $K_M$ increases to 1.2 mM.

[5] We note that DNA could not be added to saturation because of significant inner filter effects. The results must therefore be interpreted with caution.

protein tryptophans is unrestricted in both the ligand-free dimer and the binary AXP·dimer complex. In contrast, access of acrylamide to protein tryptophans is severely restricted in the binary DNA·dimer complex. Interestingly, however, all of the adenosine nucleotides (except AMP) reverse the effects of DNA; that is, DNA strongly influences $K_{SV}$ in the absence of nucleotides but not in their presence. As noted above, nucleotides *do not* affect DNA binding *affinity* (monitored by fluorescence quenching), and we interpret the ensemble of data as follows (Figure 7). First, we propose that DNA binds to gpNu1-A55 proximate to one or more tryptophan residues in the dimer, which directly quenches tryptophan fluorescence (static quenching). We suggest that the relevant residue is Trp22, which is located within the recognition helix of the wHTH motif (Figure 1B). Further, DNA binding to the nucleotide-free protein restricts the access of acrylamide to tryptophan, which influences dynamic quenching of fluorescence by acrylamide. We cannot say at present whether this is due to a conformational change in dimer structure or direct occlusion of tryptophan residues by DNA. Second, we propose that nucleotides bind to gpNu1-A55 and induce a conformational change in the dimer structure. This putative conformational change does not affect DNA binding affinity or static quenching of Trp22 by the bound DNA. We propose that the conformational change reorients the subunits across the dimer interface, which allows unrestricted acrylamide access to tryptophan residues, even in the presence of bound DNA. Thus, dynamic quenching by acrylamide is unaffected by DNA when nucleotides are present. Finally, we propose that ATP and ADP induce slightly different conformations of the gpNu1-A55 dimer (Figure 7). Structural studies (NMR and crystallography) are currently underway in our laboratory to test the hypothesis that nucleotides and DNA alter the structure of gpNu1-A55, and to define the nature of these changes at atomic resolution.

*Summary and Biological Significance*. The fluorescence-monitored ligand binding studies indicate that gpNu1-A55 retains both DNA and nucleotide binding activities. Further, the data indicate that the dimer binds nucleotides at two equivalent binding sites with high cooperativity. Neither simpler nor more complex models adequately explain the data, and the ATP binding model presented in Scheme 1 is most appropriate at present. This is consistent with the symmetric gpNu1 dimer structure determined in biophysical and structural studies. The data suggest that nucleotides induce a conformational change in the dimer, and we propose that this reflects a change in the orientation of the subunits at the dimer interface, as shown in Figure 7. Importantly, ADP binding quenches the intrinsic tryptophan fluorescence, but ATP does not; this indicates that the two nucleotides interact in subtly different ways and/or induce slightly different conformations of the dimer. A description of these subtle differences at the molecular level must await the results of structural studies currently underway in our laboratory.

Of what biological significance are the observed results? We have suggested that nucleotide hydrolysis at the gpNu1 ATPase site (i) regulates the assembly of the packaging machinery at *cos*, (ii) regulates the stability of the terminase subunits in the prepackaging complex, and (iii) modulates the transition from a stable prepackaging complex to a mobile DNA-packaging motor (*23*, *24*). In this model, the nucleotide hydrolytic cycle acts as a molecular switch, in a manner analogous to a G-protein-regulated process (*38*). The data presented here support the hypothesis that ATP and ADP stabilize different conformations of gpNu1. Recent biophysical studies in our lab indicate that a stable terminase protomer is assembled from one gpA protein in association with a gpNu1 dimer (i.e., a $gpA_1$·$gpNu1_2$ heterotrimer) (*10*). These studies further indicate that the heterotrimer self-associates into a higher-order complex, likely a ring structure. Becker and co-workers have demonstrated that ATP dramatically affects the DNase protection pattern of terminase bound to *cos* DNA (*39*), and we propose that the nucleotide binding interactions described here play a key role in regulating the assembly of a ring motor complex from the heterotrimer in vivo. We further suggest that nucleotides regulate the transition from a stable initiation complex to a mobile motor complex that translocates DNA into the capsid. A molecular description of this process must await biochemical, kinetic, and structural studies, which are currently underway in our lab.

## REFERENCES


1. Catalano, C. E. (2005) Viral Genome Packaging Machines: An Overview, *in Viral Genome Packaging Machines: Genetics, Structure, and Mechanism* (Catalano, C. E., Ed.) Landes Biosciences, Georgetown, TX.
2. Black, L. W. (1989) DNA packaging in dsDNA bacteriophages, *Annu. Rev. Microbiol. 43*, 267−292.
3. Fields, B. N., Knipe, D. M., and Howley, P. M. (1996) *Fields Virology*, 3rd ed., Lippincott-Raven Publishers, Philadelphia.
4. Becker, A., and Murialdo, H. (1990) Bacteriophage lambda DNA: The beginning of the end, *J. Bacteriol. 172*, 2819−2824.
5. Catalano, C. E., Cue, D., and Feiss, M. (1995) Virus DNA packaging: The strategy used by phage lambda, *Mol. Microbiol. 16*, 1075−1086.
6. Catalano, C. E. (2000) The terminase enzyme from bacteriophage lambda: A DNA-packaging machine, *Cell. Mol. Life Sci. 57*, 128−148.
7. Feiss, M., and Catalano, C. E. (2005) Bacteriophage Lambda Terminase and the Mechanism of Viral DNA Packaging, in *Viral Genome Packaging Machines: Genetics, Structure, and Mechanism* (Catalano, C. E., Ed.) Landes Biosciences, Georgetown, TX.
8. Gold, M., and Becker, A. (1983) The bacteriophage lambda terminase. Partial purification and preliminary characterization of properties, *J. Biol. Chem. 258*, 14619−14625.
9. Tomka, M. A., and Catalano, C. E. (1993) Physical and kinetic characterization of the DNA packaging enzyme from bacteriophage lambda, *J. Biol. Chem. 268*, 3056−3065.
10. Maluf, K. M., Yang, Q., and Catalano, C. E. (2005) Self Association Properties of the Bacteriophage Lambda Holoenzyme: Implications for the DNA Packaging Motor, *J. Mol. Biol. 347*, 523−542.
11. Furth, M. E., and Wickner, S. H. (1983) Lambda DNA Replication, in *Lambda II* (Hendrix, R. W., Roberts, J. W., Stahl, F. W., and Weisberg, R. A., Eds.) pp 145−155, Cold Spring Harbor Laboratory Press, Plainview, NY.
12. Rubinchik, S., Parris, W., and Gold, M. (1994) The in vitro ATPases of bacteriophage lambda terminase and its large subunit, gene product A. The relationship with their DNA helicase and packaging activities, *J. Biol. Chem. 269*, 13586−13593.
13. Parris, W., Rubinchik, S., Yang, Y. C., and Gold, M. (1994) A new procedure for the purification of the bacteriophage lambda terminase enzyme and its subunits. Properties of gene product A, the large subunit, *J. Biol. Chem. 269*, 13564−13574.
14. Rubinchik, S., Parris, W., and Gold, M. (1995) The in vitro translocase activity of lambda terminase and its subunits. Kinetic and biochemical analysis, *J. Biol. Chem. 270*, 20059−20066.
15. Woods, L., Terpening, C., and Catalano, C. E. (1997) Kinetic analysis of the endonuclease activity of phage lambda terminase: Assembly of a catalytically competent nicking complex is rate-limiting, *Biochemistry 36*, 5777−5785.
16. Woods, L., and Catalano, C. E. (1999) Kinetic characterization of the GTPase activity of phage lambda terminase: Evidence for

communication between the two "NTPase" catalytic sites of the enzyme, *Biochemistry 38*, 14624−14630.
17. Rubinchik, S., Parris, W., and Gold, M. (1994) The in vitro endonuclease activity of gene product A, the large subunit of the bacteriophage lambda terminase, and its relationship to the endonuclease activity of the holoenzyme, *J. Biol. Chem. 269*, 13575−13585.
18. Hang, Q., Woods, L., Feiss, M., and Catalano, C. E. (1999) Cloning, expression, and biochemical characterization of hexahistidine-tagged terminase proteins, *J. Biol. Chem. 274*, 15305−15314.
19. Yang, Q., and Catalano, C. E. (1997) Kinetic characterization of the strand separation ("helicase") activity of the DNA packaging enzyme from bacteriophage lambda, *Biochemistry 36*, 10638−10645.
20. Yang, Q., Hanagan, A., and Catalano, C. E. (1997) Assembly of a nucleoprotein complex required for DNA packaging by bacteriophage lambda, *Biochemistry 36*, 2744−2752.
21. Tomka, M. A., and Catalano, C. E. (1993) Kinetic characterization of the ATPase activity of the DNA packaging enzyme from bacteriophage lambda, *Biochemistry 32*, 11992−11997.
22. Hwang, Y., Catalano, C. E., and Feiss, M. (1996) Kinetic and mutational dissection of the two ATPase activities of terminase, the DNA packaging enzyme of bacteriophage lambda, *Biochemistry 35*, 2796−2803.
23. Yang, Q., and Catalano, C. E. (2004) A minimal kinetic model for a viral DNA packaging machine, *Biochemistry 43*, 289−299.
24. de Beer, T., Fang, J., Ortega, M., Yang, Q., Maes, L., Duffy, C., Berton, N., Sippy, J., Overduin, M., Feiss, M., and Catalano, C. E. (2002) Insights into specific DNA recognition during the assembly of a viral genome packaging machine, *Mol. Cell 9*, 981−991.
25. Yang, Q., Berton, N., Manning, M. C., and Catalano, C. E. (1999) Domain structure of gpNu1, a phage lambda DNA packaging protein, *Biochemistry 38*, 14238−14247.
26. Yang, Q., de Beer, T., Woods, L., Meyer, J. D., Manning, M. C., Overduin, M., and Catalano, C. E. (1999) Cloning, expression, and characterization of a DNA binding domain of gpNu1, a phage lambda DNA packaging protein, *Biochemistry 38*, 465−477.
27. Bain, D. L., Berton, N., Ortega, M., Baran, J., Yang, Q., and Catalano, C. E. (2001) Biophysical characterization of the DNA binding domain of gpNu1, a viral DNA packaging protein, *J. Biol. Chem. 276*, 20175−20181.
28. Frackman, S., Siegele, D. A., and Feiss, M. (1985) The terminase of bacteriophage lambda. Functional domains for *cosB* binding and multimer assembly, *J. Mol. Biol. 183*, 225−238.
29. Kypr, J., and Mrazek, J. (1986) Lambda phage protein Nu1 contains the conserved DNA binding fold of repressors, *J. Mol. Biol. 191*, 139−140.
30. Becker, A., and Gold, M. (1988) Prediction of an ATP reactive center in the small subunit, gpNu1, of the phage lambda terminase enzyme, *J. Mol. Biol. 199*, 219−222.
31. Gill, S. C., and von Hippel, P. H. (1989) Calculation of protein extinction coefficients from amino acid sequence data, *Anal. Biochem. 182*, 319−326.
32. Gill, S. C., and von Hippel, P. H. (1990) Calculation of Protein Extinction Coefficients from Amino Acid Sequence Data, *Anal. Biochem. 189*, 283.
33. Lakowicz, J. R. (1983) *Principles of fluorescence spectroscopy*, Plenum Press, New York.
34. Lakowicz, J. R. (1999) *Principles of fluorescence spectroscopy*, 2nd ed., Kluwer Academic/Plenum, New York.
35. Burstein, E. A., Vedenkina, N. S., and Ivkova, M. N. (1973) Fluorescence and the location of tryptophan residues in protein molecules, *Photochem. Photobiol. 18*, 263−279.
36. Babbar, B. K., and Gold, M. (1998) ATP-reactive sites in the bacteriophage lambda packaging protein terminase lie in the N-termini of its subunits, gpA and gpNu1, *Virology 247*, 251−264.
37. Flowers, S., Biswas, E. E., and Biswas, S. B. (2003) Conformational dynamics of DnaB helicase upon DNA and nucleotide binding: Analysis by intrinsic tryptophan fluorescence quenching, *Biochemistry 42*, 1910−1921.
38. Bhattacharya, M., Babwah, A. V., and Ferguson, S. S. G. (2004) Small GTP-Binding Protein-Coupled Receptors, *Biochem. Soc. Trans. 32*, 1040−1044.
39. Higgins, R. R., and Becker, A. (1995) Interaction of terminase, the DNA packaging enzyme of phage lambda, with its *cos* substrate, *J. Mol. Biol. 252*, 31−46.

BI050333E